Estuarine, Coastal and Shelf Science 302 (2024) 108765

Contents lists available at ScienceDirect

Estuarine, Coastal and Shelf Science

journal homepage: www.elsevier.com/locate/ecss

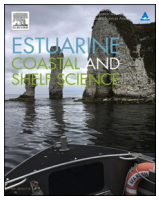

Hydrodynamics and wave transmission through a hollow triangle breakwater

Tu Le Xuan [a,**], Hoang Thai Duong Vu [b,*], Peter Oberle [b], Thanh Duc Dang [c], Hoang Tran Ba [a], Hung Le Manh [a]

[a] Southern Institute of Water Resources Research, Ho Chi Minh City, Viet Nam
[b] Karlsruhe Institute of Technology (KIT), Institute for Water and Environment (IWU), Kaiserstraße 12, 76131, Karlsruhe, Germany
[c] Department of Civil and Environmental Engineering, University of South Florida, Tampa, USA

ARTICLE INFO

Keywords:
Mekong delta
Hollow triangle breakwater (TC1)
Hydrodynamics
Wave transmission
Wave forces
FLOW-3D

ABSTRACT

Coastal protection, shoreline stabilization and mangrove forest restoration are pressing issues in such coastal regions worldwide as the Mekong Delta. A hollow triangle breakwater TC1 was developed to protect the coastline against erosion. The TC1 breakwater consists of holes arranged on the waveward and leeward sides, allowing for wave energy dissipation, water exchange, and sediment deposition to facilitate mangrove restoration. To evaluate comprehensively the working principles of the TC1, we investigate herein the wave-structure interaction under regular waves by means of an advanced computational fluid dynamics (CFD) platform, i.e. FLOW-3D. The numerical model was calibrated against experimental results with great agreement across three different water depths where the breakwater was tested. We also analyzed the velocity dynamics in the waveward and leeward sides of the breakwater and it revealed a significant difference of approximately 50% following the change in water depths from 0.66 m to 0.96 m. Furthermore, we examined the wave forces on both solid and hollow forms of TC1 structures, the wave forces on a hollow form were found to decrease by 20–30% in comparison with the forces on a solid form. In addition, the effect of liquid characteristics, i.e., density, viscosity and temperature showed slightly impact on wave transmission coefficients through the breakwater by 0.4–0.7 %.

1. Introduction

The Mekong Delta is a crucial region for food security not only for Vietnam but also the world (Vu et al., 2022a; Trinh et al., 2014). However, the delta is facing an increasing vulnerability due to flooding (Schenk et al., 2022; Vu et al., 2021; Nestmann et al., 2016), land subsidence (Minderhoud et al., 2019), hydropower dam construction (Hecht et al., 2019), sediment reduction (Le Xuan et al., 2019), river bank erosion, salinity intrusion, and coastal erosion (Le Xuan et al., 2022b). Currently, the coastal shoreline along the Mekong Delta is eroding with a rate of 20–50 m per year, which is among the most serious challenges to sustainable development of the region (Le Xuan et al., 2022b). As a result, many types of breakwater structures have been developed and built along the coast of the delta, such as geotube, semi-circular breakwater, pile-rock breakwater, hollow triangle breakwater, and curtain wall breakwater (Le Xuan et al., 2019; Tuan et al., 2022; Le Xuan et al., 2022a). However, many failure examples of breakwaters were documented due to soft soil foundation in the Mekong Delta (Vu et al., 2022b; Minh et al., 2020; Le Xuan et al., 2022b).

Previously, numerous studies employed laboratory experimental approaches to assess the hydrodynamic behavior of wave transmission (van der Meer and Daemen, 1994; Van der Meer, 1995; Oumeraci et al., 2001) and fluid-structure interaction, wave reduction efficiency as well as the stability of breakwaters (Oumeraci and Partenscky, 1991; Suh et al., 2006; Muttray et al., 2007; Liu et al., 2016). For example, Dhinakaran et al. (2008, 2009), Hee Min Teh et al. (2012) studied wave-structure interactions, hydraulic pressures, and wave forces on a hollow semi-circular breakwater under irregular waves. Lyu et al. (2020) investigated the wave transmission and forces on a submerged partially semi-circular breakwater. They pointed out that an increasing porosity by about 12% significantly decreased wave reflections and horizontal forces. Similarly, Li et al. (2020) also suggested that the porosity of 8–15% was recommended in the design of quarter-circular breakwaters. Besides, Dao et al. (2020) performed an experimental

* Corresponding author.
** Corresponding author.
E-mail addresses: xuantutl@gmail.com (T. Le Xuan), hoang.vu@kit.edu (H.T.D. Vu).

https://doi.org/10.1016/j.ecss.2024.108765
Received 8 January 2024; Received in revised form 18 March 2024; Accepted 12 April 2024
Available online 14 April 2024

evaluation on the flow resistance of wooden fences in the coast of Vietnam. Tuan et al. (2022) studied wave transmission and wave damping of a porous breakwater on mangrove mudflats.

In response to the serious coastal erosion in the Mekong Delta, the Southern Institute of Water Resources Research (SIWRR), Vietnam developed a new structure called "hollow triangle breakwater - TC1". This structure has been implemented along the Mekong coast, e.g. in Tien Giang province, with a length of 7.0 km since 2019 (see Fig. 1). The TC1 was tested by means of physical modelling in 2018 (Le Xuan et al., 2022a). This hollow structural breakwater is a component of "Multiple Lines of Defense Strategy" coastal protection solutions aimed at restoring mangrove forests and coastal ecosystems. It is one of natural-based solutions that combine engineering and non-engineering solutions to adapt to sea level rise and climate change proposed by Le Xuan et al. (2022b). Fig. 1 shows a section of the perforated breakwater TC1 constructed along the coast of Mekong Delta. It can be seen that, since building in 2019, the breakwaters have been successful in sediment trapping and mangrove species have gradually recovered in the protected area.

During the experimental investigation Le Xuan et al. (2022a), a complete hydraulic characterization of the TC1 was not possible regarding time and costs; therefore, to have a comprehensive understanding of such working principles of the TC1 in terms of wave transmission, velocity field, turbulent kinetic energy and wave forces need further investigation.

Computational fluid dynamics (CFD) tools, e.g. FLOW-3D, have been applied widely in hydraulic design (Song and Vu, 2012), sediment transport (Kosaj et al., 2022), flow resistance of vegetation (Fard, 2020), and flood management (Gems et al., 2016). In addition, FLOW-3D has been worldwide applied and demonstrates a high capacity for simulating wave interaction with coastal structures (Bayon et al., 2016; Monfort et al., 2019; Le Quéré et al., 2020). Recently, Vu et al. (2022) examined wave transmission through configurations of curtain wall breakwaters under variable conditions in the Mekong Delta based on this numerical code. Buccino et al. (2019a,b) applied this CFD platform to simulate the loading process on a sloping top caisson breakwater subjected to significant overtopping. Besides, Gomes et al. (2020) applied FLOW-3D to study the stability of a semi-circular breakwater on a rubble mound foundation. The application of this CFD in the field of coastal and ocean engineering is recently growing and proved rather efficient in describing the loading process at monolithic coastal structures, even under breaking waves (Buccino et al., 2019a). On the other hands, several studies on wave damping by porous structures, i.e., wooden and bamboo fences, sand evolution, sediment transport and dampers using other numerical modelling, e.g., SWASH, 2DH, Particle Swarm Optimization, were carried out by Dao et al. (2018); Dao et al. (2021); Pourzangbar and Maurizio (2022); and Pourzangbar and Mostafa (2021).

The estuaries and coastal area of the Mekong Delta are dominated by the sediment and discharge of the Mekong River, the flow density changes when mixing by salt water from the sea, fresh water and sediment from the Mekong river (Wolanski et al., 1996; Horner-Devine et al., 2015; Le Xuan et al., 2019; Hecht et al., 2019; Eslami et al., 2021). It is costly to analyze the influence of these factors on wave transmission through the hollow breakwater in the laboratory given the complexity of phenomena to be reproduced and the amount of needed measurements. Hence, it is more convenient to apply a numerical approach to investigate the effect of different fluid characteristics, i.e., fresh water, salt water, and salt water with high sedimentation concentration on wave transmission coefficients through the breakwaters.

The objective of this paper is to investigate the wave-structure interaction on the hollow triangle breakwater regarding wave transmission, velocity field, turbulent kinetic energy, and hydraulic pressure in numerical approach. Then, we examined wave forces on a hollow breakwater in comparison with a solid form. Finally, we investigated the effect of fluid characteristics change on wave transmission coefficients through a hollow breakwater in numerical model, which would require considerable preparation works and cost to be investigated in the laboratories.

The paper is structured as follows: In section 2, the methodology is presented to describe the principles of wave-structure interaction, CFD model description, geometry and boundary condition. The results are presented and discussed in section 3. Finally, the conclusions are provided in section 4.

2. Methodology

2.1. Principles of wave-structure interaction

When waves impact on a breakwater, a part of the wave energy is reflected toward the structure, a part is dissipated or absorbed by the breakwater, and a proportion is transmitted through the breakwater (Fig. 2). Theoretically, this phenomenon obeys the law of conservation of energy and can be expressed as follows:

$$E_i = E_t + E_r + E_d \quad (1)$$

In which, E_i, E_t, E_r, and E_d are the energy of the incident wave, transmission wave, reflected wave, and the dissipated energy, respectively.

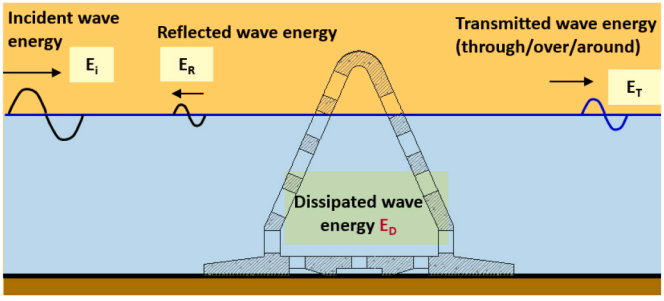

Fig. 2. Sketch of wave energy components through TC1 breakwater.

Fig. 1. A section of hollow triangle breakwater TC1 constructed along the coast of Mekong Delta (pictures taken in 2023).

According to Le Xuan et al. (2022a), this energy balance function can be normalized and rewritten as:

$$1 = \left(\frac{H_t}{H_i}\right)^2 + \left(\frac{H_r}{H_i}\right)^2 + \frac{E_d}{E_i} \quad (2)$$

$$1 = K_t^2 + K_r^2 + K_d^2 \quad (3)$$

In which:

$K_t = \frac{H_t}{H_i}$ is the wave transmission coefficient which is determined by the ratio of the height of the transmitted wave through the structure (H_t), towards the leeward of this, and the height of the incident wave in the waveward side of the structure (H_i); $K_r = \frac{H_r}{H_i}$ is the wave reflection coefficient, which is determined by the ratio between the height of the reflected wave (H_r) over the height of the incident wave (H_i), both measured in the waveward side of the structure;

The wave dissipation coefficient (K_d), is determined equating expression (3):

$$K_d^2 = 1 - K_t^2 - K_r^2 \quad (4)$$

2.2. CFD model description

FLOW-3D, a computational fluid dynamics software package developed by *Flow Science Inc* (Flow 3D, 2009), is a *state-of-the-art* tool with a high capacity to simulate fluid dynamics problems. It solves the transition Navier-Stokes equations averaged over a volume-of-fluid (VOF method). Several modelling options exist to integrate into the numerical solver the properties of flow turbulence at scales smaller than the averaging domain. These include Prandtl's mixing length theory, one-equation turbulent energy (k), two-equation turbulent energy (k-ε), Renormalized Group (RNG), and Large Eddy Simulation (LES) models.

2.3. Geometry and boundary condition

2.3.1. Model setup

The dimension of the breakwater used in this research follows the experimental design of the TC1 breakwater described in Le Xuan et al. (2022a) and Minh et al. (2022). The wave flume in the numerical approach was setup exactly as the experimental 1:7 scale test, which followed Froude similitude. The wave flume in the laboratory at the SIWRR has a total length of 34 m, a height of 1.4 m, and a width of 1.2 m. The flume was divided into three zones (Fig. 3), including deep water area near a long wave generator with a length of 3 m; a 10 m transitional zone with a slope of 1/25 and a long shoal zone of 16 m. At the end of the flume, there was a wave absorber with a length of 5 m. The flume was manufactured with glasses on the sides and a smooth steel plate at the bottom with the Manning's roughness coefficient in range of 0.01–0.012, respectively to minimize the friction and roughness of the sides and flume bed.

Fig. 3 shows the arrangement of wave gauges and the geometry of the breakwater in the numerical model. The breakwater is placed at 21 m far from the wave maker, Rc is the freeboard crest to evaluate the submerged rate of the structure corresponding to different water depths (d). Besides, four wave gauges (WG1-WG4) were installed in the deep water zone (D) to measure the reflect water due to the transition slope following the recommendation by Masard and Funke (1980), and WG5 was placed in front of the structure. WG6 was setup in the leeward of the structure TC1 to measure the transmitted wave passing through the breakwater, WG7 was placed in front of the wave absorbed zone. In addition, there are two sensors of E40 to measure the velocity, and they are placed at the same positions of WG5 and WG6.

The computational domain is covered with a meshing block covering the entire domain with constant sized hexahedral cells ($\Delta x = \Delta y = \Delta z$), mesh refinement and convergence analysis followed recommendations by Celik et al. (2008); liquid properties included water at 20 °C, density of 1000 kg/m^3, dynamic viscosity of 0.001 kg/m/s; time-step was controlled by "Stability and convergence" and automatically adapted in order to ensure that Courant–Friedrichs–Lewy (CFL) numbers remained below a threshold of 0.45; advection was discretized by using a second order scheme while the fluid fraction is solved with the default Volume of Fluid (VOF) scheme (Hirt and Nichols, 1981).

FLOW-3D can simulate regular linear and nonlinear waves (Stokes, Stokes and Cnoidal, and Solitary) as well as random or irregular waves. Here, random waves represent the natural sea state with the wave spectra of JONSWAP or Pierson-Moskowitz, respectively. In this study, we applied regular waves to investigate the working principles of the TC1 in terms of wave transmission, velocity field, turbulent kinetic energy and wave forces.

2.3.2. Boundary conditions

Table 1 shows the boundary conditions for investigating the wave transmission through porous and solid breakwaters with different wave characteristics and water depths. The range of wave heights, wave periods and water depths corresponding to the actual wave oscillation and tidal variations at the coastal areas of the Mekong Delta (Zemann et al., 2023). Table 2 shows the range of input parameters/choices which were considered to find optimal parameters in the numerical setup enabling the reproduction of the experimental investigation. The choice of the

Table 1
Boundary conditions for simulation.

Type of breakwater	H (m)	T (s)	D (m)	Rc (m)
TC1	0.1; 0.15	1.5; 1.89; 2.27	0.96	−0.15
	0.1; 0.15	1.5; 1.89; 2.27	0.86	−0.05
	0.07; 0.15	1.5; 1.89; 2.27	0.81	0
	0.07; 0.15	1.5; 1.89; 2.27	0.76	0.05
	0.07; 0.15	1.5; 1.89; 2.27	0.71	0.1
	0.07; 0.1; 0.15	1.5; 1.89; 2.27	0.66	0.15
Solid	0.15	1.5	0.96	−0.15
	0.15	1.5	0.86	0.0
	0.15	1.5	0.66	+0.15

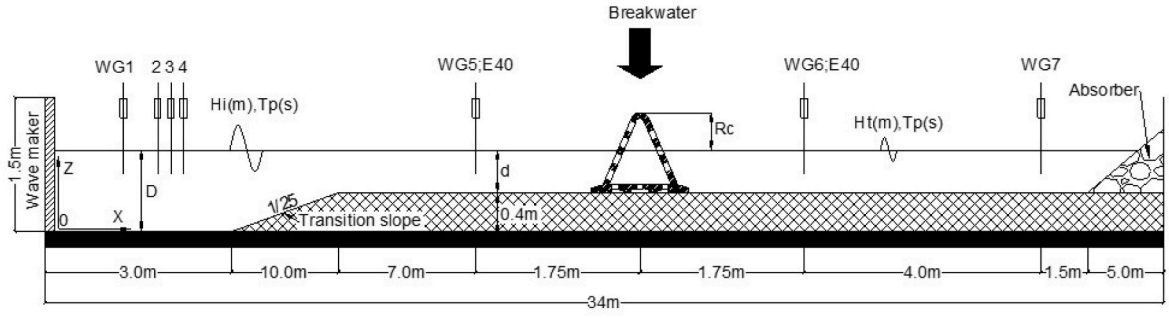

Fig. 3. Wave gauges and structure arrangement in numerical and physical wave flume.

Table 2
Input parameters for numerical verification.

Depth (m)	Wave H (m); T (m)	Meshing size (m)	Turbulence model	Surface roughness Ks (m)
0.66; 0.81; 0.96	0.15 m; 1.5 s	0.02, 0.015, 0.01, 0.005	k-e, k-w, RNG, LES	0.02; 0.005; 0.002; 0

turbulence model is not a calibration procedure, since their choice depends rather on the type and scale of results which are targeted; in the present investigation, both RANS and LES were tested since in the case study both could confer satisfactory results and to infer the potential costs of such future investigations.

In the first step, numerical approach was calibrated with experimental results to examine wave transmission through the structure. This calibration serves as the main parameterization to obtain the main investigation results. Then, due to the change of fluid characteristics and sediment transport in the monsoon seasons in the Mekong Delta (Unverricht et al., 2014), parameterization corresponding to different fluid characteristics are investigated to evaluate the effect on the wave transmission through the breakwater (Table 3). The simulation time was chosen to be 60 s as the waves should be of near permanent form and the height of the waves from one cycle to the next within the examined duration should have minimum prescribed fluctuations for an acceptable regular wave (Brekke and Chakrabarti, 2005). Therefore, we analyzed the waves in the most stable interval of around 10 waves from 20 s to 40 s and the recording time for data analysis was setup of 10 Hz (0.1 s) in the numerical model.

3. Results and discussions

3.1. Model verification

3.1.1. A sensitivity analysis of input parameters in numerical model

In a first step, a sensitivity study of wave transmission coefficient through the breakwater due to the change of grid size, roughness parameterization, and turbulence models in numerical approach was performed for the case of shallow water depth D = 0.66 m, wave height H = 0.15 m and wave period T = 1.5 s. The wave transmission coefficients (Kt) through the breakwater are shown in Table 4, it can be seen that the grid size plays hence a significant change of wave transmission coefficients in numerical simulation results. In contrast, the surface roughness in the numerical model plays a minor impact on the result. The best value of wave transmission coefficients (Kt) of numerical simulations is 0.46, which is closest with experimental result of 0.47 through TC1 was obtained when using LES as turbulence model, for a grid side of 0.01 m or 0.005 m, and a surface roughness $K_s = 0$ m (surface roughness is neglected).

Next, the parameterization including grid size of 0.01 m, turbulence model LES, and Ks = 0 m were selected for model verification and further investigation. Fig. 4 shows a great agreement between the results of numerical model (CFD, blue circular) with experimental data (EXP, red rectangular) regarding wave transmission coefficients (Kt) versus the ratio of crest freeboard and incoming wave heights (Rc/Hi). Specifically, the Kt values of numerical results shows a great agreement in cases of submerged states (D = 0.81m and 0.96m corresponding to Rc/Hi = 0 and −1), at the emerge state (D = 0.66 m corresponding to Rc/Hi = 1), the wave transmission coefficient Kt in numerical model shows slightly lower due to higher broken waves at the shallow water depth. Figure S3 and Figure S6 in the Supplementary Material show detailed comparison of surface water elevations at the wave gauges (WG5, WG6, WG7) between numerical and physical models for the case of shallow water (D = 0.66 m), while Figs. S1, S2, S4, S5 illustrate further the comparison of free surface elevations at water depths of D = 0.81 m and D = 0.96 m.

Table 3
Different liquids for wave transmission investigation.

Description	Temperature (°C)	Viscosity (kg/m/s)	Density (kg/m^3)
Liquid 1: fresh water	20	0.00100	1000
Liquid 2: salt water	20	0.00126	1020
Liquid 3: salt water and sediments	20	0.00126	1050

3.1.2. Comparison of velocity between numerical and experimental results

After validation the numerical model in term of wave transmission coefficients, we examined further the comparison of velocity at the sensor E40 (Fig. 3) between numerical and physical results for the cases of No structure and the TC1 to enhance the accuracy of numerical approaches.

Fig. 5 illustrate the comparison of velocity at WG6 between the simulation results for the cases of without a breakwater (left) and with the TC1 (right). The comparison results show that the numerical model performed well in the case without a breakwater and especially for intermediate and deep water (D ≥ 0.81 m). In the case of TC1 and shallow water (D = 0.66 m), acceptable results were obtained. Additionally, RMSE and CC indexes show an acceptable range of comparison between CFD and laboratory results in term of velocity measurement, see Figs. S7–S8 in the Supplementary Materials. Therefore, this enhances the accuracy of numerical simulation results.

3.2. Effect of wave characteristics on wave transmission coefficients

Previous studies such as Le Xuan et al. (2022a) and Minh et al. (2022) examined the wave transmission coefficients through the TC1 only under random waves in the laboratory and did not consider regular waves. Therefore, this study is necessary to supplement the transmission coefficients under regular waves in numerical modelling to have a comprehensive investigation on wave transmission coefficients through this breakwater.

Fig. 6 shows the relationship between wave transmission coefficient K_t versus the relative crest freeboard (Rc/Hi) between numerical simulation and experimental results under regular and irregular waves. The experimental data of irregular waves were collected from previous research by Le Xuan et al. (2022a) and Minh et al. (2022). The comparison results indicated that there was not a significant difference in the wave transmission coefficient (Kt) between regular (blue circle) and irregular (green triangle) waves. For the cases of the submerged breakwater ($R_c/H_i < 0.0$ m) and equal to the water surface Rc/Hi = 0.0 m, there was a relatively large wave transmission coefficient with K_t values ranging from 0.6 to 0.8 and the wave reduction efficiency was less than 50%. The case of the emerging breakwater Rc/Hi > 0.0 had a higher wave dissipation efficiency than the case of the submerged breakwater. However, in case of Rc/Hi > 1, the wave reduction is very small, because the waves mainly passed through the holes inside the breakwater body and less overtopping on the breakwater crest. When the crest freeboard Rc/Hi in the range of 1–3, the wave transmission coefficients have the lowest values Kt = 0.3–0.45 corresponding to the wave reduction of more than 50%. The effect of crest freeboard on the wave transmission coefficients is consistent with the findings of the earlier study by Dhinakaran (2011), Teh et al. (2012), Le Xuan et al. (2022a), and Minh et al. (2022).

3.3. Investigate the velocity change in the leeward and waveward sides of the structure

3.3.1. The evolution of velocity fields

Fig. 7 shows the wave development and movement through the hollow breakwater for different instants from 14.7 s to 15.0 s for the case of D = 0.71 m, H = 0.15 m, T = 1.5 s. When the wave impacted the

Table 4
Results of sensitivity analysis of wave transmission coefficients in numerical simulations (CFD) and experimental test (EXP).

No	Approach	H (m)	T (s)	D (m)	Turbulence model	Grid size (m)	Ks (m)	Kt
1	CFD	0.15	1.5	0.66	LES	0.02	0	0.53
2	CFD	0.15	1.5	0.66	LES	0.015	0	0.49
3	CFD	0.15	1.5	0.66	LES	0.01	0	0.46
4	CFD	0.15	1.5	0.66	LES	0.005	0	0.46
5	CFD	0.15	1.5	0.66	LES	0.01	0.002	0.45
6	CFD	0.15	1.5	0.66	LES	0.01	0.005	0.45
7	CFD	0.15	1.5	0.66	LES	0.01	0.02	0.44
8	CFD	0.15	1.5	0.66	k-e	0.01	0	0.52
9	CFD	0.15	1.5	0.66	RNG	0.01	0	0.51
10	CFD	0.15	1.5	0.66	Laminar	0.01	0	0.44
11	EXP	0.15	1.5	0.66				0.47

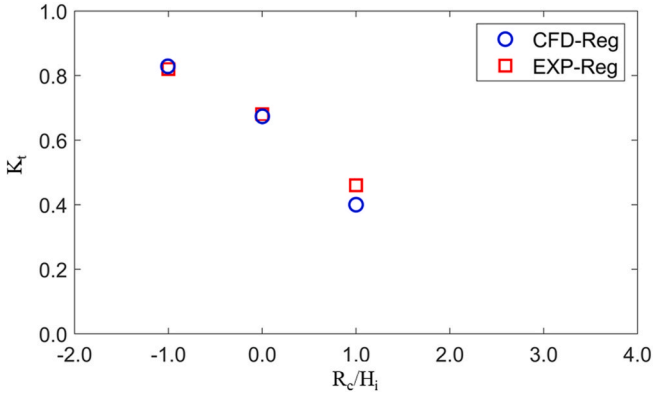

Fig. 4. Comparison of wave transmission coefficients between numerical simulation (CFD) and experimental (EXP) results.

breakwater, a part of the wave was reflected back to the waveward side, a part of the wave was dissipated inside the breakwater, and a part was transmitted to the leeward region. There was a great variation in the value and the distribution according to depth when waves acted on the breakwater in different time steps from t = 14.7 s to t = 15.0 s. The distribution of the velocity values passing in and out of the structure. This clarifies the wave dissipation mechanism and the change in velocity when the wave interacts with the hollow breakwater.

In the waveward region of the structure: Waves produced the largest horizontal flow velocity and distributed over the surface layer with depth from (0–0.4)d showing a great velocity 0.3–0.5 m/s, while the velocity decreases from middle to the bottom (0.4–1.0)d, (velocity is about 0.25 m/s), this increases the possibility of sediment transport from the sea to the rear of the structure.

Inside the structure: The arrangement of holes and the shape of the breakwater influenced the values and velocity distribution inside the breakwater. When waves passed through rows of holes arranged evenly on the entire surface in the waveward of the breakwater, the velocity increased significantly (greater than 0.5 m/s), and the direction tended to be towards the bottom of the structure. After that, the wave hit the back surface of the structure, creating turbulence inside the breakwater. A part of waves passed through rows of holes on the back to the shore side. Holes on the backside were arranged higher than the bottom of the breakwater and tended to move toward the face for an upwelling effect. The turbulence process of waves inside the breakwater accommodated conditions to stir up sediment carried from the sea to the shore, at the same time creating the process of enriching oxygen for water and increasing nutrients and sediment deposition for the area in the leeward of the breakwater.

In the leeward of the structure: Due to the hollow breakwater dissipating wave energy and changing the direction of velocity, the

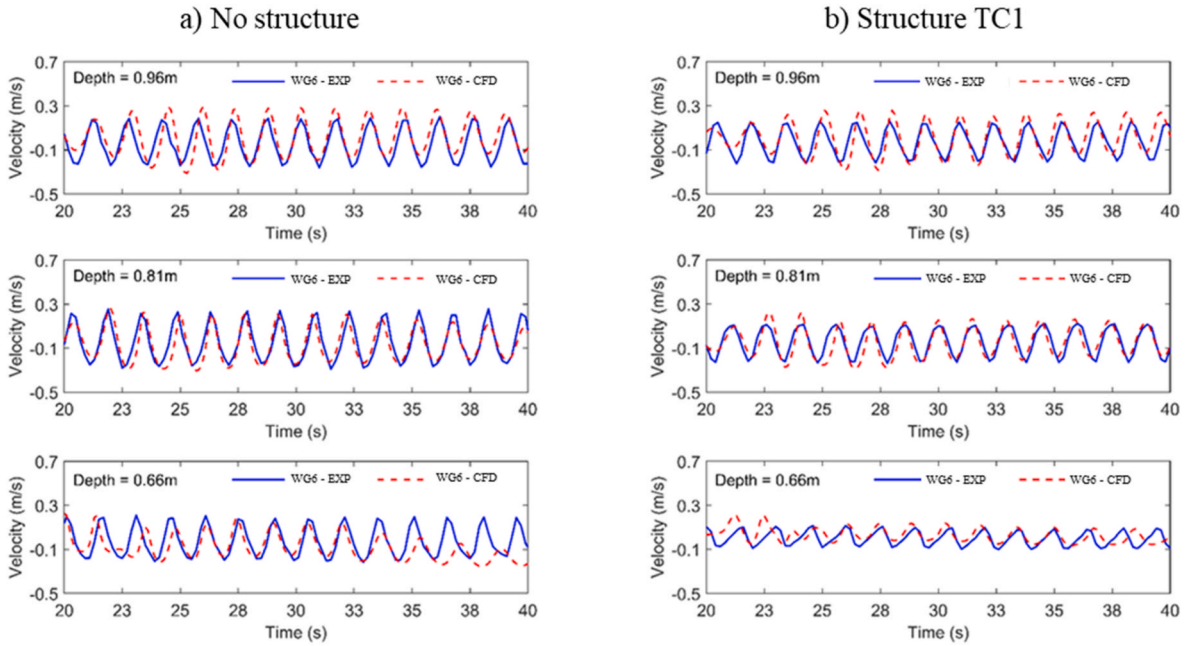

Fig. 5. Comparison of velocity (a, b) at WG6 for the cases of No structures (left) and with TC1 (right) between numerical (CFD) and experimental results (EXP).

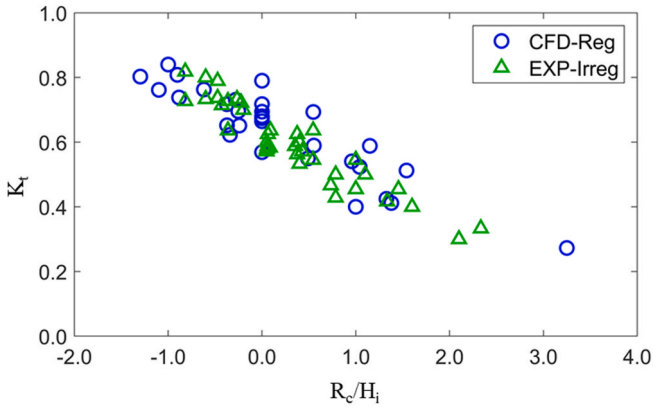

Fig. 6. Wave transmission coefficients through the TC1 under regular (CFD-Reg) and random waves (EXP-Irreg).

distribution of the velocity field after the structure changed significantly and markedly reduced compared with the velocity in the waveward of the structure. This is shown by the velocity distribution on the longitudinal section, at the surface layer corresponding to the depth (0–0.2) d the flow velocity maintains quite large from 0.25 to 0.5 m/s. In the middle layer and the bottom layer (0.2–1.0)d, the flow velocity decreased sharply (smaller than 0.25 m/s). At the bottom layer (0.8–1.0) d, the velocity was very small.

The interaction process of waves and currents with this breakwater through many holes in both sides may change velocity, turbulence patterns and direction of bottom current that contributes to the nutrient enrichment of the water body, thus attracting biological species (Kim and Kim, 2013). The enrichment of water oxygenation facilitates coastal habitats to live inside or near the leeward of the breakwater (Pickering and Whitmarsh, 1997).

3.3.2. *Investigate the velocity change in the leeward and waveward sides of the structure*

Two points at WG5 and WG6 were examined to investigate the velocity changes in different water levels for two cases of no structures (left) and with structure TC1 (right), see Fig. 8. The results show that when the water level increased from 0.66 to 0.96 m, the average velocity increased significantly from 0.1 m/s to 0.2 m/s. In the case without of breakwater, the velocity values at WG5 and WG6 were almost the same; but there was a significant change in velocity at these two locations corresponding to the water depth of 0.66 m and 0.81 m for the case of with structure, the velocity at WG5 increased significantly while the velocity at WG6 decreased. For the case of shallow water (Rc = + 0.15 m), the velocity at WG5 was 0.12 m/s as twice the velocity at WG6. This shows that when the structure worked in shallow water, the current was dissipated relatively large through the holes in the waveward and in the leeward sides of the breakwater. When the water level increased to the crest of the breakwater (Rc = 0 m), the velocity at WG5 increased up to 0.24 m/s and the velocity behind the WG6 was 0.15 m/s. This shows that when the water level increased, the wave overtopping of the breakwater and breaking partly and due to reflected waves that caused the velocity at WG5 to be higher and the velocity at WG6 also increased significantly. When Rc = - 0.15 m, the breakwater was completely submerged. The waves passed mostly through the top of the breakwater and the waves were less dissipated. As a result, the velocity values at WG5 and WG6 were relatively similar, but the average value of velocity was also higher than the velocity in the case of the breakwater working in shallow water.

3.4. *Turbulent kinetic energy distribution*

Fig. 9 shows the distribution of turbulent kinetic energy (TKE)

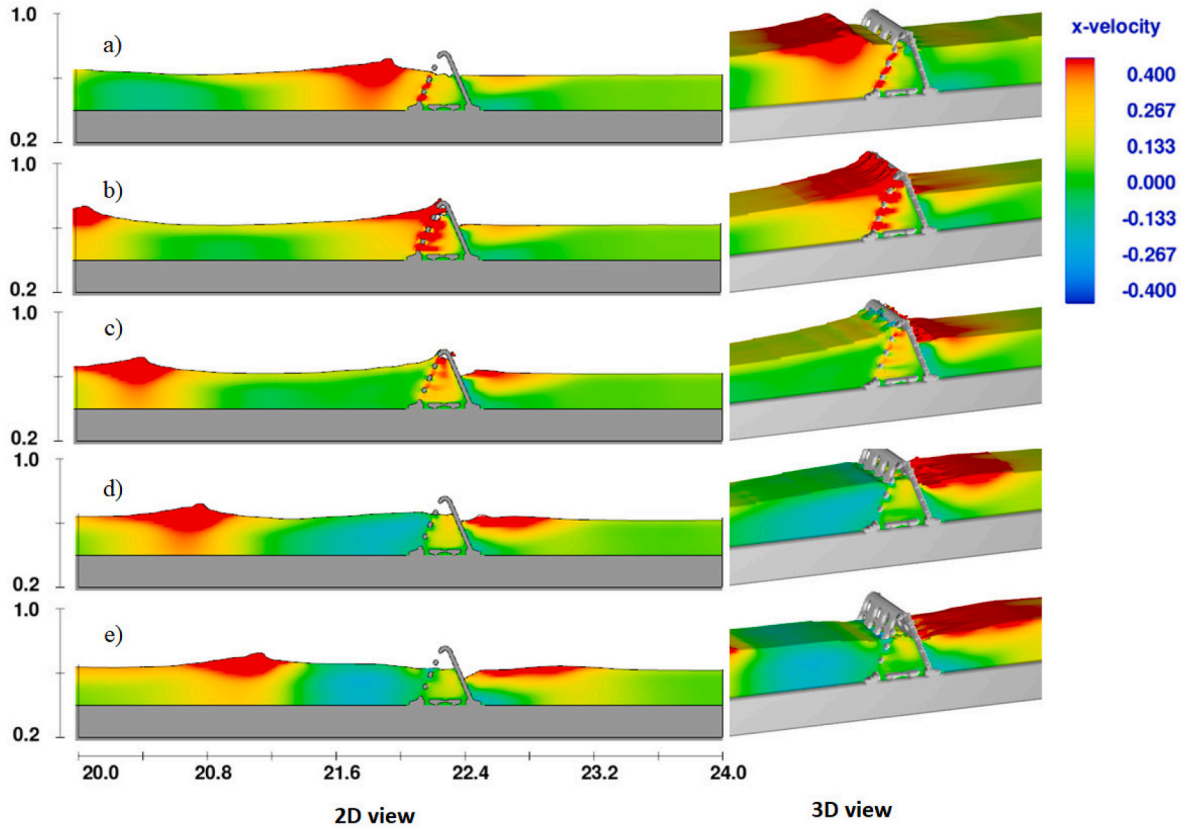

Fig. 7. Velocity field in (x, z) direction from t = 14.7 s (a) to t = 15.0 s (e) in the case of water depth of 0.71 m.

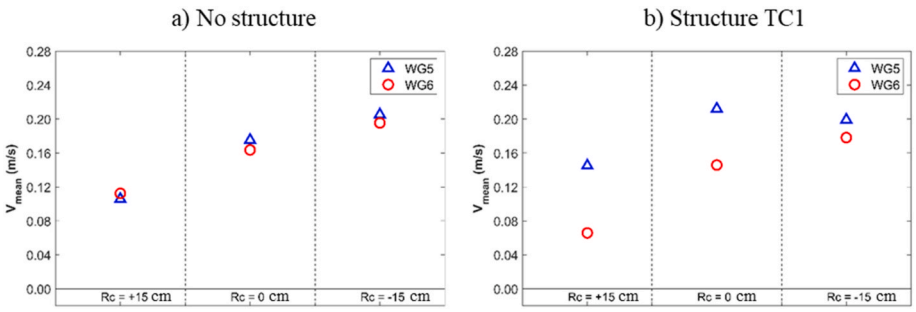

Fig. 8. Average velocity at WG5 and WG6 in three cases Rc = + 0. 15 m; 0 m; - 0.15 m, without structures (left) and with TC1 (right).

generated in the case of D = 0.71, H = 0.15, T = 1.5 s. The turbulent energy concentrated at the crest of the wave, and it decreased when the waves pass through the breakwater. Fig. 11 shows the dissipation of turbulent energy dissipation at the position of the wave contacting and passing through the breakwater. The largest part of wave energy was at the crest with the maximum value of 0.005 (J/kg). The process of dissipation of turbulent energy is closely related to the process of changing flow velocity due to waves when interacting with hollow structures. When passing through a hollow breakwater, in case of low velocity, energy loss in this case is due to viscous friction between moving fluid layers. However, when the flow velocity increases and the perforated hollow structure has a large enough cavity size, flow turbulence will be created inside. The flow through the perforated hollow structure is a turbulent flow, the Darcy Forchheimer motion resistance causes the gradual increase of the linear and nonlinear resistance coefficients that reduces the flow velocity inside the hollow structure, wave energy, then the wave height also decreases accordingly.

When interacting with the body surface of the breakwater, a part of the turbulent energy that passes through the holes inside the body of the breakwater and dissipates there. The divergence of the wave in several

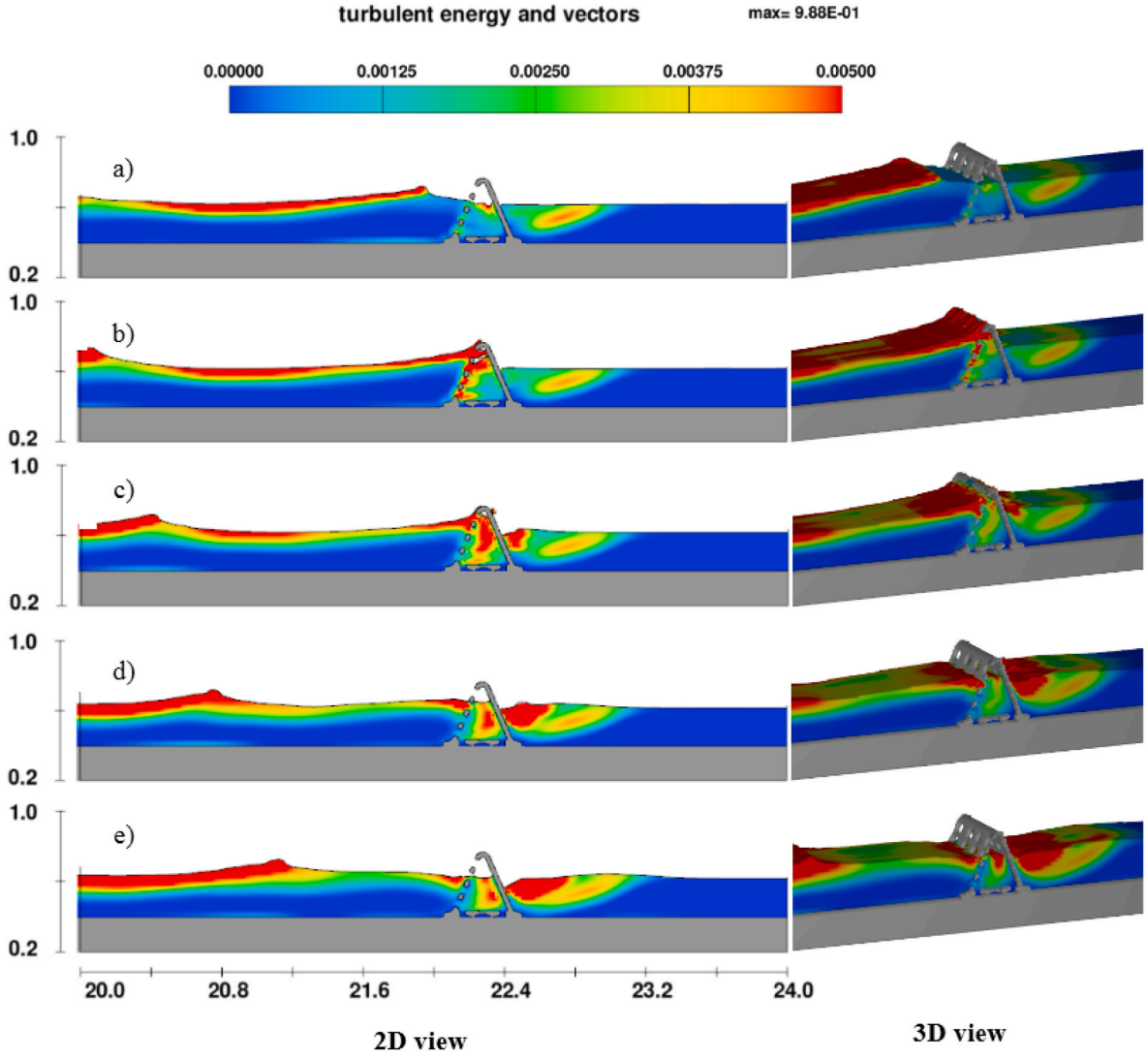

Fig. 9. Turbulent Kinetic Energy distribution from t = 14.7 s (a) to t = 15.0 s (e).

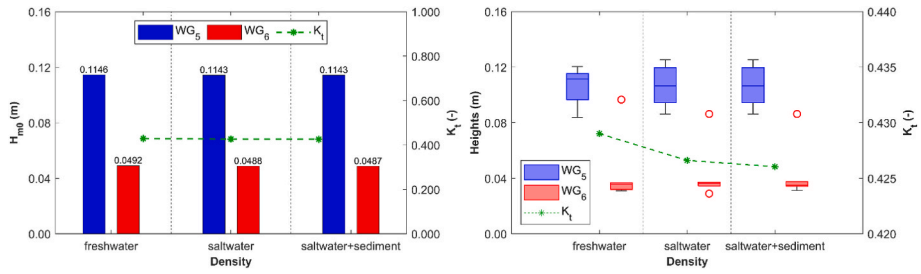

Fig. 10. Effect of changes in the fluid viscosity and density due to changes in the fluid (fresh water, brine and brine with suspended sediments) on the wave transmission.

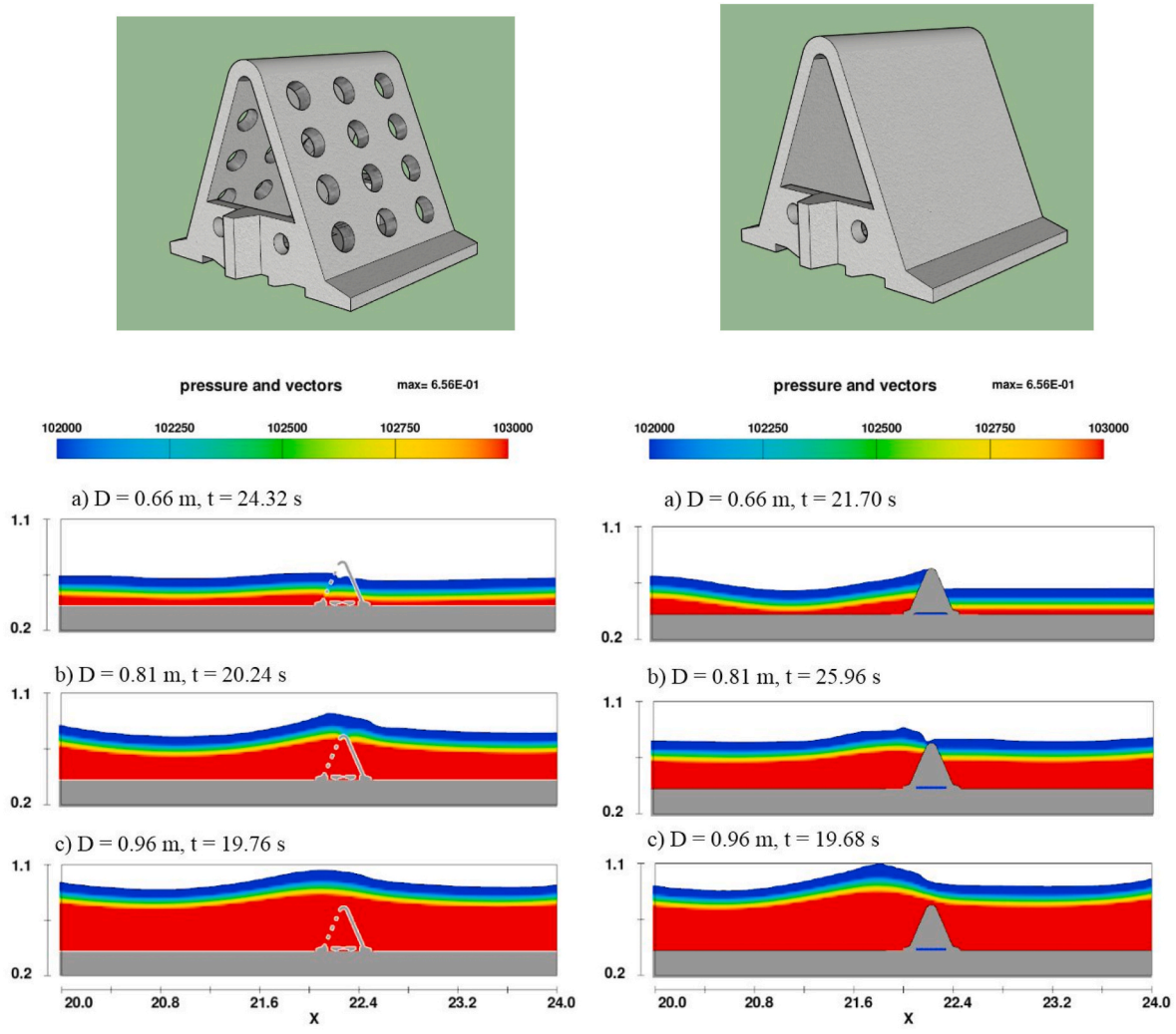

Fig. 11. Pressure distribution at different time steps on TC1 and Solid structures corresponding to three water depths.

jet flumes through the perforated surface, increases the turbulent production due to dispersion and creation of multiple shear layers. This turbulence production is made at the cost of mean energy loss, favoring the dissipation of the wave energy. It can be seen that the turbulent energy of the wave was mostly dissipated here and the remaining energy after passing through the hole layers also interacted with each other and dissipated in the leeward of the breakwater.

Similar to velocity distribution, TKE carried a relatively large value on the surface because the waves moved with high speed in this layer. When the wave impacted on a hollow breakwater, TKE was very large. Inside the body of the breakwater, there was a very large TKE, and this dissipated the wave energy. When the wave passed through the breakwater body, a large amount of wave energy was dissipated right in the leeward of the structure, especially near the water surface, and this effect gradually decreased toward the bottom. The red areas in Fig. 9 are the locations where TKE has the largest energy dissipation from 0.0025 to 0.005 J/kg. This is also in-line with the study by Gomes et al. (2020) on semi-circular breakwaters.

3.5. *Effect of fluid characteristics on wave transmission coefficients through the breakwater*

As shown in Fig. 10, the effect of liquid characteristics (viscosity and density) on wave transmission coefficients were investigated for regular

waves with H = 0.15 m and T = 1.15 s, corresponding to three different cases in Table 3 (fresh water, saltwater and salt water with suspended sediments). The wave transmission coefficient through TC1 changed very slightly in the range of 0.426–0.428 corresponding to three liquid characteristics oscillating. It was noticed that an increase in liquid density causes a slightly decrease in wave transmission. As liquid density increases from 1000 to 1050 kg/m3 corresponding to an increase of 2.0–3.4%, the Kt values decrease from 0.47 to 0.7%.

In the context of changes in flow and sediment from the upstream of the Mekong River, studies by Horner-Devine et al. (2015), Le Xuan et al. (2019), and Sepehr Eslami et al. (2021) have shown the mixing process of fresh, saltwater and decrease sediment discharged into the sea. However, these factors have little effect on wave transmission. However, this type of breakwater has an advantage of maintaining good environmental exchange between the offshore and the nearshore area, exchanging saltwater and freshwater environments, and trapping sediment from the Mekong River as well as the inherent coastal sources that have been accumulating in the continental shelf (Oanh et al., 2002). This is essential in exchange of fine sediment (Tuan et al. (2022)), maintaining nutrient supplies for mangrove forests and fisheries to maintain mangrove forests and ecosystem (Kim and Kim, 2013; Pickering and Whitmarsh, 1997).

3.6. Comparison of wave force on the hollow and solid forms of TC1

Fig. 11 illustrates the wave pressures distribution on different forms of TC1 (surface hollow form, left) and Solid (solid form, right). Similar wave input conditions (H = 0.15 m; T = 1.5s) and three different depths (D = 0.66 m; D = 0.81 m; and D = 0.96 m) were simulated for two types of structures to compare the pressure distribution along the wave flumes for two structural forms. The simulated pressure in FLOW-3D included atmospheric pressure of 101,325 Pa.

The horizontal forces on two different forms of TC1 were illustrated in Fig. 12. The simulation results show that in the three simulated water depths, the cases of low water depth D = 0.66 m and high water depth D = 0.96 m showed the smallest impact forces and the case of water depth equal to the crest of the structure D = 0.81 m showed a large value of force on the structure. The force on the structure in case of hollow structure was reduced by nearly 25–30% compared to the case of solid structure. This was consistent with the studies by Oumeraci et al. (1993) in case of the reduction of pressures on a hollow sheet and consistent with Dhinakaran et al. (2008), Teh et al. (2012), Gomes et al. (2020) in case of reduction of pressures on a semi-circular breakwater. Particularly, the case of D = 0.66 m and D = 0.96 m, the force on the structure was quite similar, respectively 36.65 N and 36.87 N on TC1 and 49.8 N and 49.2 N on the solid structure, the difference of horizontal forces between TC1 and Solid was approximately 25–26%. In the case D = 0.81 m, the horizontal force on the structure was largest. It was 41.53 N for TC1 and 59.15 N in the case of Solid (Fig. 12d). The different forces on TC1 and Solid due to the Solid form created a phase difference in pressure in the leeward and waveward sides of the structure, so the difference in horizontal forces on Solid was larger than that in the case of the TC1 (Fig. 11). In addition, Fig. 12a, b, c illustrate the time shift of the peak wave force is caused by the interaction of the wave-structure interaction, as well as wave reflection. Therefore, corresponding to different water levels, this process will undergo variations, resulting in changes in the time of maximum force impact in different simulation scenarios. This shows that hollow breakwater form had an advantage of reducing the force on the structure, increasing the stability of the structure and reducing the construction materials in comparison with a solid form.

These advantages are especially important when the structure is built on soft-soil and weak foundation, such as in the coastal areas of the Mekong Delta as it reduces construction costs due to less weight of the structure. The foundation treatment is also simpler, and the construction process is faster because the precast components are easy to assemble. Additionally, environment exchange before and in the leeward of the porous breakwater is also better than the solid one.

4. Conclusions

This study examined a comprehensive investigation of wave-structure interaction on a hollow triangle breakwater TC1 based on numerical approach (FLOW-3D) under regular waves. The simulation results were consistent with the results from the physical model in terms of wave transmission coefficients and velocity at different water depths. Furthermore, with the numerical investigation it was capable to devise further in-depth knowledge on the interaction of these structures with waves. We found that owing to the influence of the arrangement of holes, when the wave passes through, the wave energy was dissipated significantly.

The TC1 works effectively with more than 50% of wave energy dissipation in the emergence state corresponding to low water depth of 0.66 m. When the breakwater was in the submerged states (D = 0.81 m and 0.96 m), the wave damping efficiency reduced and was in range of 20–30%. Similarity, the velocity distribution in the waveward and leeward sides of the structure corresponding to different water depths D = 0.66 m, 0.81 m, and 0.96 m shows that when the structure worked in the emergence state Rc ≥ 0, the velocity induced by waves transmitted through the structure was significantly reduced by more than 50%.

The wave forces on the TC1 structure were smaller in comparison with the case of the solid structure by 20–30 %. This finding shows the less requirement for stability of a hollow breakwater in foundation treatment under soft-soil conditions and reduces less amount of construction materials for pre-casting works.

The effect of fluid characteristics on wave transmission coefficients through the TC1 are minor. It is noticed that an increase of liquid density due to high sediment concentration during the monsoon seasons caused

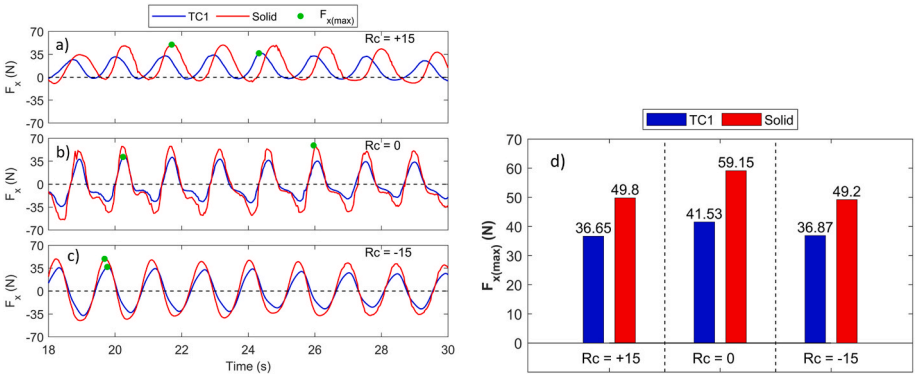

Fig. 12. Comparison of wave forces on hollow and solid forms of TC1 corresponding to different water depths.

a slightly decrease in wave transmission. As liquid densities increased from 1000 1050 kg/m^3, the Kt values decrease from 0.47 to 0.7 %.

It is important to address that, the hollow triangle breakwater TC1 is designed not to completely eliminate waves but maintain a certain amount of waves transmitted through the breakwater for ecological system and sediment deposition. Hence, the TC1 can create favorable conditions for the exchange of water environment and sediment. It increases sediment trapping in the leeward of the breakwater that facilitate the growth of mangroves as well as aquatic species in the coastal area.

CRediT authorship contribution statement

Tu Le Xuan: Conceptualization, Data curation, Formal analysis, Investigation, Methodology, Software, Validation, Writing – original draft, Writing – review & editing. **Hoang Thai Duong Vu:** Supervision, Software, Resources, Methodology, Investigation, Formal analysis, Data curation, Conceptualization, Validation, Visualization, Writing – original draft, Writing – review & editing. **Peter Oberle:** Project administration, Writing – review & editing. **Thanh Duc Dang:** Writing – original draft, Writing – review & editing. **Hoang Tran Ba:** Supervision. **Hung Le Manh:** Supervision.

Declaration of competing interest

The authors declare that they have no known competing financial interests or personal relationships that could have appeared to influence the work reported in this paper.

Data availability

Data will be made available on request.

Acknowledgements

The work presented in this publication was performed within the framework of the ViWaT project which is sponsored by the German Federal Ministry for Education and Research (BMBF) and partially supported by the Ministry of Science and Technology (MOST) Vietnam.

Acronyms and symbols

VMD	Vietnamese Mekong Delta
SIWRR	Southern Institute of Water Resources Research
WG	Wave Gauge
E40	Velocity speed measured gauge
CFD	Computational fluid dynamics
R_c	Crest freeboard (m)
Rc/H	Relative crest freeboard
H	Wave height (m)
Hi	Incident wave height (m)
Ht	Transmitted wave height (m)
K_t	Wave transmission coefficient
K_r	Wave reflection coefficient (−)
K_d	Wave energy dissipation coefficient (−)
E_i	Energy of incident wave
E_t	Energy of transmitted wave
E_r	Energy of reflected wave
E_d	Energy of dissipated wave
D	Depth in wave flume near the wave maker (m)
d	Depth in front of the breakwater (m)
T	Wave period (s)
η	Free surface elevation (m)
V	Velocity (m/s)
F_x	Horizontal forces on TC1 (N)

Appendix A. Supplementary data

Supplementary data to this article can be found online at https://doi.org/10.1016/j.ecss.2024.108765.

References

Bayon, A., Valero, D., García-Bartual, R., López-Jiménez, P.A., 2016. Performance assessment of OpenFOAM and FLOW-3D in the numerical modeling of a low Reynolds number hydraulic jump. Environ. Model. Software 80, 322–335.

Brekke, J., Chakrabarti, S., 2005. Chapter 9 –Drilling and production risers. In: Handbook of Offshore Engineering, pp. 709–859. https://doi.org/10.1016/B978-0-08-044381-2.50016-3.

Buccino, M., Daliri, M., Dentale, F., Calabrese, M., 2019a. CFD experiments on a low crested sloping top caisson breakwater. Part 2. Analysis of plume impact. Ocean Eng. 173, 345–357.

Buccino, M., Daliri, M., Dentale, F., Di Leo, A., Calabrese, M., 2019b. CFD experiments on a low crested sloping top caisson breakwater. Part 1. nature of loadings and global stability. Ocean Eng. 182, 259–282.

Celik, I.B., Ghia, U., Roache, P.J., 2008. Procedure for estimation and reporting of uncertainty due to discretization in CFD applications. J. Fluid Eng. 130 (7), 1–4. https://doi.org/10.1115/1.2960953.

Dao, T., Stive, M.J.F., Hofland, B., Mai, T., 2018. Wave damping due to wooden fences along mangrove coasts. JCR (J. Coast. Res.) 34 (6), 1317–1327. https://doi.org/10.2112/JCOASTRES-D-18-00015.1, 2018.

Dao, H.T., Hofland, B., Stive, M.J.F., Mai, T., 2020. Experimental assessment of the flow resistance of coastal wooden fences. Water 12 (7), 1910. https://doi.org/10.3390/w12071910.

Dao, H.T., Hofland, B., Suzuki, T., Stive, M.J.F., Mai, T., Tuan, L.X., 2021. Numerical and small-scale physical modelling of wave transmission by wooden fences. Journal of Coastal and Hydraulic Structures 1. https://doi.org/10.48438/jchs.2021.0004.

Dhinakaran, G., Sundar, V., Sundaravadivelu, R., Graw, K.U., 2008. Hydrodynamic characteristics of seaside perforated semi-circular breakwaters due to random waves. J. Waterw. Port, Coast. Ocean Eng. 134 (4), 237–251.

Dhinakaran, G., Sundar, V., Sundaravadivelu, R., Graw, K.U., 2009. Effect of perforations and rubble mound height on wave transformation characteristics of surface piercing semi-circular breakwaters. Ocean Eng. 36 (15–16), 1182–1198.

Eslami, S., Hoekstra, P., Minderhoud, P.S.J., et al., 2021. Projections of salt intrusion in a mega-delta under climatic and anthropogenic stressors. Commun Earth Environ 2, 142. https://doi.org/10.1038/s43247-021-00208-5.

Fard, A.R.T., 2020. Influence of vegetation on shear stress and flow rate in open channel using FLOW-3D. In: CERJ, 9. https://doi.org/10.19080/CERJ.2020.09.555774.

Flow 3D, 2009. FLOW-3D User Manual V9, 3.

Gems, B., Mazzorana, B., Hofer, T., Sturm, M., Gabl, R., Aufleger, M., 2016. 3D-hydrodynamic Modelling of Flood Impacts on a Building and Indoor Flooding Processes. https://doi.org/10.5194/nhess-2015-326.

Gomes, A., Pinho, J.L., Valente, T., Antunes do Carmo, J.S., V Hegde, A., 2020. Performance assessment of a semi-circular breakwater through CFD modelling. J. Mar. Sci. Eng. 8 (3), 226.

Hecht, J.S., Guillaume, L., Mauricio, E.A., Thanh, D.D., Thanapon, P., 2019. Hydropower dams of the Mekong River basin: a review of their hydrological impacts. In: Journal of Hydrology, 568, pp. 285–300. https://doi.org/10.1016/j.jhydrol.2018.10.045.

Hirt, C.W., Nichols, B.D., 1981. Volume of fluid (VOF) method for the dynamics of free boundaries. In: Journal of Computational Physics, 39, pp. 201–225. https://doi.org/10.1016/0021-9991(81)90145-5.

Horner-Devine, A.R., Hetland, R.D., MacDonald, D.G., 2015. Mixing and transport in coastal river plumes. Annu. Rev. Fluid Mech. 47, 569–594.

Kim, D.-S., Kim, M.C., 2013. The changes in marine environment and biological community in sea areas around an artificial upwelling structure during the summer. Anim. Cell Syst. 17, 357–365.

Kosaj, R., Alboresha, R.S., Sulaiman, S.O., 2022. Comparison between numerical Flow3d software and laboratory data, for sediment incipient motion. IOP Conf. Ser. Earth Environ. Sci. 961 (1), 12031. https://doi.org/10.1088/1755-1315/961/1/012031.

Le Quéré, P.A., Nistor, I., Mohammadian, A., 2020. Numerical modeling of tsunami-induced scouring around a square column: performance assessment of FLOW-3D and Delft3D. J. Coast Res. 36 (6), 1278–1291.

Le Xuan, T., Vo, Q.T., Johan, R., Song, P.V., Tran, A.D., Thanh, D.D., Dano, R., 2019. Sediment transport and morphodynamical modeling on the estuaries and coastal zone of the Vietnamese Mekong Delta. In: Continental Shelf Research, 186, pp. 64–76. https://doi.org/10.1016/j.csr.2019.07.015.

Le Xuan, T., Le, M.H., Tran, B.H., Do, v.d., Vu, H.T.D., Wright, D., et al., 2022a. Wave energy dissipation through a hollow triangle breakwater on the coastal Mekong Delta. In: Ocean Engineering, 245, 110419. https://doi.org/10.1016/j.oceaneng.2021.110419.

Le Xuan, T., Hoang, T.B., Vo, Q.T., Wright, D., Tanim, H., Duong, T.A., 2022b. Evaluation of coastal protection strategies and proposing multiple lines of defense under climate change in the Mekong Delta for sustainable shoreline protection. Ocean Coast Manag. 228, 106301.

Li, A.J., Liu, Y., Liu, X., Zhao, Y., 2020. Analytical and experimental studies on water wave interaction with a submerged perforated quarter-circular caisson breakwater. Appl. Ocean Res. 101, 102267.

Liu, Y., Li, H.J., Zhu, L., 2016. Bragg reflection of water waves by multiple submerged semi-circular breakwaters. Appl. Ocean Res. 56, 67–78.

Lyu, Z., Liu, Y., Li, H., Mori, N., 2020. Iterative multipole solution for wave interaction with submerged partially perforated semi-circular breakwater. Appl. Ocean Res. 97, 102103.

Masard, E.P.D., Funke, E.R., 1980. The measurement of incident and reflected spectra using a least squares method. Incicent and reflected spectra.

Minderhoud, P.S.J., Coumou, L., Erkens, G., Middelkoop, H., Stouthamer, E., 2019. Mekong delta much lower than previously assumed in sea-level rise impact assessments. In: Nature Communications, 10, p. 3847. https://doi.org/10.1038/s41467-019-11602-1, 1.

Minh, N.N., Dinh, C.S., Duong, D.V., Nestmann, F., Zemann, M., Vu, H.T.D., Dan, T.C., 2020. Evaluating the effectiveness of existing coastal protection measures. In: Mekong Delta, pp. 1419–1429. https://doi.org/10.1007/978-981-15-0291-0_192.

Minh, N.N., Duong, D.D., Duy, T.L., San, D.C., Nhat, T.P., Quyen, N., Bang, T., Wright, D., Tanim, H., Duong, T.A., 2022. Wave reduction efficiency for three classes of breakwaters on the coastal Mekong Delta. Appl. Ocean Res. 129 (December 2022), 103362.

Monfort, C.L., Fenical, S., Riley, R., Watson, N., 2019. CFD wave loading and response analysis for large interconnected float systems. In: Ports 2019: Port Engineering. American Society of Civil Engineers, Reston, VA, pp. 44–54.

Muttray, M., Oumeraci, H., Oever, E.T., 2007. Wave reflection and wave run-up at rubble mound breakwaters. In: Coastal Engineering 2006, 5, pp. 4314–4324.

Nestmann, F., Trinh, C.V., Vu, H.T.D., Oberle, P., Hinz, S., Geiger, H., 2016. Geographical impact of dyke measurement for land use on flood water in the Mekong Delta. Available online at: https://www.researchgate.net/publication/303370408.

Oanh, T.T.K., Lap, N.V., Tateishi, M., Kobayashi, I., Tanabeb, S., Saito, Y., 2002. Holocene delta evolution and sediment discharge ofthe Mekong River, southern Vietnam. Quat. Sci. Rev. 21, 1807–1819.

Oumeraci, H., Partenscky, H.W., 1991. Wave-induced pore pressure in rubble mound breakwaters. In: Coastal Engineering, 1990, pp. 1334–1347.

Oumeraci, H., Klammer, P., Partenscky, H.W., 1993. Classification of breaking wave loads on vertical structures. J. Waterw. Port, Coast. Ocean Eng. 119 (4), 381–397.

Oumeraci, H., Kortenhaus, A., Allsop, W., de Groot, M., Crouch, R., Vrijling, H., Voortman, H., 2001. Probabilistic Design Tools for Vertical Breakwaters. CRC Press.

Pickering, H., Whitmarsh, D., 1997. Artificial reefs and fisheries exploitation: a review of the 'attraction versus production' debate, the influence of design and its significance for policy. Fish. Res. 31, 39–59.

Pourzangbar, A., Mostafa, V., 2021. Optimal design of brace-viscous damper and pendulum formatted: justified tuned mass damper using particle swarm optimization. Appl. Ocean Res. 112, 102706. ISSN 0141-1187. https://doi.org/10.1016/j.apor.2021.102706.

Pourzangbar, A., Maurizio, B., 2022. A new process-based, wave-resolving, 2DH circulation model for the evolution of natural sand bars: The role of nearbed dynamics and suspended sediment transport. Coastal Eng. 177, 104192. ISSN 0378-3839. https://doi.org/10.1016/j.coastaleng.2022.104192.

Schenk, A., Oberle, P., Canh, P.N., Tran, D.D., Vu, H.T.D., Vu, H.L., 2022. Datasets of land use change and flood dynamics in the Vietnamese mekong delta. Data Brief 42. https://doi.org/10.1016/j.dib.2022.108268, 2022, 108268, ISSN 2352-3409.

Song, P.V., Vu, H.T.D., 2012. Stilling basin design in downstream of Thu Bo barrier by numerical and physical models. In: Science of Water Resources Engineering and Environment Nr, 37, pp. 6–2012.

Suh, K.D., Park, J.K., Park, W.S., 2006. Wave reflection from partially perforated-wall caisson breakwater. Ocean Eng. 33 (2), 264–280.

Teh, Hee Min, Venugopal, Vengatesan, Bruce, Tom, 2012. Performance analysis of composite semicircular breakwaters of different configurations and porosities. Coast Eng. J.

Trinh, C.V., Vu, H.T.D., Nestmann, F., Oberle, P., Nam, N.T., 2014. Land use based flood hazard analysis for the Mekong Delta. In: Proceedings of the 19th IAHR-APD Congress 2014. https://doi.org/10.13140/2.1.5153.9842. Hanoi, Vietnam.

Tuan, Q.T., Mai, T.L., Le, N.C., 2022. Laboratory study of wave damping by porous breakwaters on mangrove mudflats in the Mekong River Delta. Ocean Eng. 258, 111846 https://doi.org/10.1016/j.oceaneng.2022.111846.

Unverricht, D., Thanh, C.N., Heinrich, C., Szczuciński, W., Lahajnar, N., Stattegger, K., 2014. Suspended sediment dynamics during the inter-monsoon season in the subaqueous Mekong Delta and adjacent shelf, southern Vietnam. J. Asian Earth Sci. 79 (Part A), 509–519. https://doi.org/10.1016/j.jseaes.2012.10.008. ISSN 1367-9120.

Van der Meer, J.W., 1995. Conceptual design of rubble mound breakwaters. In: Advances in Coastal and Ocean Engineering, 1, pp. 221–315.

Van der Meer, J.W., Daemen, I.F., 1994. Stability and wave transmission at low-crested rubble-mound structures. J. Waterw. Port, Coast. Ocean Eng. 120 (1), 1–19.

Vu, H.T.D., Tran, D.D., Van, T.C., Oberle, P., Hinz, S., Nestmann, F., 2021. Evaluating the impacts of rice-based protection dykes on floodwater dynamics in the Vietnamese mekong delta using geographical impact factor (GIF). In: Water, 13, p. 1144. https://doi.org/10.3390/w13091144, 9.

Vu, H.T.D., Schenk, A., Tran, D.D., Nguyen, C.P., Vu, H.L., Oberle, P., Van, T.C., Nestmann, F., 2022a. Land use change in the Vietnamese Mekong Delta: new evidence from remote sensing. In: The Science of the Total Environment, 151918. https://doi.org/10.1016/j.scitotenv.2021.151918.

Vu, H.T.D., Zemann, M., Oberle, P., Seidel, F., Nestmann, F., 2022b. Investigating wave transmission through curtain wall breakwaters under vairable conditions. Journal of Coastal and Hydraulic Structures 2, 19. https://doi.org/10.48438/jchs.2022.0019.

Wolanski, E., Huan, N.N., Nhan, N.H., Thuy, N.N., 1996. Fine-sediment dynamics in the Mekong River estuary, Vietnam. Estuarine. Coastal and Shelf Science 43 (5), 565–582.

Zemann, M., van der Linden, R., Trinh Cong, D., Vu, D.H.T., Nguyen, N.M., Seidel, F., Oberle, P., Nestmann, F., Fink, A.H., 2023. Modelling Ocean Wave Conditions at a Shallow Coast under Scarce Data Availability – A Case Study at the Western Coast of the Mekong Delta, Vietnam, EGUsphere. https://doi.org/10.5194/egusphere-2022-1447.